Available online at www.sciencedirect.com
SCIENCE DIRECT®
Journal of Catalysis 215 (2003) 177–187
JOURNAL OF CATALYSIS
www.elsevier.com/locate/jcat

The synthesis and structure of a single-phase, nanocrystalline MoVW mixed-oxide catalyst of the Mo_5O_{14} type

S. Knobl,[a] G.A. Zenkovets,[b] G.N. Kryukova,[b] O. Ovsitser,[c] D. Niemeyer,[a] R. Schlögl,[a] and G. Mestl [c,*]

[a] *Abteilung Anorganische Chemie, Fritz-Haber-Institut der Max-Planck-Gesellschaft, Faradayweg 4-6, 14195 Berlin, Germany*
[b] *Boreskov Institute of Catalysis, pr. Lavrentieva, 5, 630090 Novosibirsk, Russia*
[c] *NanoScape AG, Frankfurter Ring 193 A, 80807 Munich, Germany*

Received 21 May 2002; revised 2 October 2002; accepted 4 December 2002

Abstract

The different preparation steps are characterized for the single-phase, crystalline, ternary oxide $(MoVW)_5O_{14}$, which is important for catalytic, mild selective oxidation reactions. For the synthesis of this oxide, solutions of ammonium heptamolybdate, ammonium metatungstate, and vanadyl oxalate were spray-dried followed by different thermal treatments. The structures of the materials formed at each preparation step, starting from the precursor to the final product, were studied using scanning and transmission electron microscopy, X-ray powder diffraction, thermal analysis, and Raman spectroscopy. Raman spectroscopy was also applied to shed some light into the aqueous chemistry of the mixed precursor solutions. Raman data indicate that a molecular structure which seems to be closely related to that of the final crystalline Mo_5O_{14}-type oxide is already formed in solution. X-ray diffraction revealed that the thermal treatment steps strongly affect the degree of crystallinity of the ternary Mo_5O_{14} oxide. Transmission electron microscopy with energy-dispersive microanalysis confirmed the presence of V and W in the molybdenum oxide particles and gave evidence for the (010) plane as the most developed face of the crystals of this phase. Details of the structural transformation of this system at the different preparation and calcination steps are discussed in relation to their performance in the selective partial oxidation of acrolein to acrylic acid.

Keywords: Partial oxidation; Catalysis; MoVW mixed oxide; Synthesis; Mo_5O_{14}

1. Introduction

About one quarter of all organic products produced worldwide are synthesized via catalytic selective partial oxidation reactions. The industrial and economic relevance of research in this field, hence, is self evident. Generally, these industrial processes are highly developed. Improvements of such processes can be achieved only if fundamental understanding is reached about active catalyst structures and their relation to catalytic performance.

Currently, MoVW-supported catalysts are used in industry for the synthesis of acrylic acid [1–5]. Despite this industrial importance, fundamental information is unavailable on both the structure formation during synthesis and the peculiarities of the atomic arrangements in these systems depending on different preparation routes and element ratios.

Previously, the Mo_5O_{14}-type phase was found to be highly important for selective partial oxidation catalysis, for example methanol oxidation [6], acrolein oxidation [7], and propene oxidation [8]. Proceeding work [6–9] showed that the selectivity for partial oxidation products could be considerably augmented when the amount of Mo_5O_{14} was increased. The structure of this oxide is built up by pentagonal bipyramids and octahedrally coordinated metal centers [10]. Coordination sphere changes that might explain its activity in partial oxidation catalysis can easily be imagined in this structure. This oxide forms at a definite transition metal ratio of Mo:V:W equal to 0.68:0.23:0.09. At the same time binary molybdenum-based oxides doped with different elements such as Nb, W, and Ta have been synthesized and their structures have been identified as those of the Mo_5O_{14} type [11,12]. These phases were found to be

* Corresponding author.
E-mail address: gerhard.mestl@nanoscape.de (G. Mestl).

0021-9517/03/$ – see front matter
doi:10.1016/S0021-9517(03)00006-X

stable at a wide temperature range and a broad variation of the element ratios. However, the ternary system has not yet been synthesized as a single-phase material without traces of other molybdenum oxides; e.g., thermal treatment in inert atmosphere results in the appearance of MoO_2, while treatment in air leads to MoO_3.

Its identification as an important phase for partial oxidation catalysis makes this $(MoVW)_5O_{14}$ oxide also important as a model substance for fundamental surface science studies, provided that single crystals could be grown. Attempts to grow single crystals via gas-phase transport reactions or sintering [8,13,14] showed that this phase forms from mixtures of molybdenum and tungsten and from mixtures of molybdenum, tungsten, and vanadium, but not from binary Mo–V mixtures with high V concentrations. Both tungsten and vanadium play important roles as structural promoters in the formation and stabilization of this oxide and hence for catalytic activity.

It seems plausible that different thermal treatments of the precursor solutions affect (a) the composition of the usually mixed-phase catalysts and (b) the crystal sizes of the different constituting phases. Thus, the understanding of the aqueous precursor chemistry is required to control the preparation of such mixed-oxide catalysts. Furthermore, subsequent drying and activation procedures from the liquid precursor to the active and selective catalyst are of paramount importance for the development of the optimum catalytic performance. Accordingly, knowledge has to be generated about the detailed processes which occur during these synthesis steps. Only then might it be possible to fully control not only the phase composition of the mixed-oxide catalyst, but also the crystal size, the crystallinity, and the morphology of the active phase. A developed synthesis routine thus could lead to defined crystal sizes or even nanocrystalline $(MoVW)_5O_{14}$ mixed-oxide catalysts. Moreover, it offers a versatile path to control its elementary composition. Effects of crystallite size/morphology and elemental composition on the catalytic performance could be studied separately.

To this end, some steps of the developed aqueous preparation procedure are characterized by in situ micro Raman spectroscopy. The important subsequent drying process and further activation and formation procedures are investigated by in situ Raman spectroscopy, high-resolution electron microscopy (HREM), and X-ray diffraction (XRD). Comparison with Raman spectra of well-defined, single-crystalline reference oxides [13] was used to assign the obtained spectra during these catalyst preparation routes to certain oxides, such as MoO_2, Mo_4O_{11}, Mo_8O_{23}, MoO_3, or Mo_5O_{14}.

This investigation was aimed at the preparation of a single-phase Mo_5O_{14}-type material and the study of its molecular architecture at every step of the synthesis. Possible changes of the particle morphologies of the ternary oxide and its precursors during thermal treatment were also the focus of this study. Last but not least, the detected physical alterations during synthesis should be related to the changing catalytic activity and selectivity in the partial oxidation of acrolein.

This approach of a knowledge-based development of all synthesis steps combined with the use of complementary physicochemical characterization techniques led to the defined preparation of a single-phase $(MoVW)_5O_{14}$ oxide catalyst for acrolein partial oxidation.

2. Experimental

The mixed-oxide catalyst with the $Mo_{0.68}V_{0.23}W_{0.09}O_x$ composition was prepared by spray-drying of mixed solutions of ammonium heptamolybdate (AHM; Merck, p.a.), ammonium metatungstate (AMT; Fluka; purum, $>85\%$ WO_3 gravimetric), and vanadyl oxalate of the respective transition metal concentrations with a pH value of 2. The aqueous solution of AHM with the concentration of 0.963 mol/L MoO_3 was prepared by dissolving AHM in bidistilled water at 353 K. The aqueous solution of AMT with the concentration of 0.271 mol/l WO_3 was prepared by dissolving AMT in bidistilled water at 353 K. The aqueous solution of vanadyl oxalate with the concentration of 0.379 mol/L was prepared by dissolving V_2O_5 (Merck; extra pure) in an aqueous solution of oxalic acid (EGA-Chemie; $>99\%$) with the concentration of 1.93 mol/L at 353 K. The different transition metal precursor solutions were allowed to cool to room temperature and then mixed by adding the corresponding amounts with a metering pipette. The mixed solutions were heated at 353 K for 1 h.

The $Mo_{0.68}V_{0.23}W_{0.09}$ oxide solid catalyst precursor was prepared by spray-drying the mixtures of the aqueous solutions of AHM, AMT, and vanadyl oxalate with a spray-dryer of the "Anhydro"-type. Subsequently, the obtained product was calcined at 623 K for 120 min in flowing air (flow rate: 3.6 L/h) and at 723 K in flowing helium (flow rate: 3.6 L/h) for 120 min or only at 713 K in flowing air for 240 min. The heating rate to these end temperatures was 6 K/min. The calcination was done in a gas flow reactor placed in a tube furnace.

The Mo, V, and W concentrations in the precursor solutions, the solid precursor, and the catalysts were determined by atomic absorption spectroscopy (Perkin–Elmer, PE 4100).

Raman spectroscopy was performed on a Labram I (Dilor) instrument equipped with a confocal microscope (Olympus). A notch filter (Kaiser Optical) was applied to cut off the laser-line and the Rayleigh scattering up to 150 cm^{-1}. The spectrometer is equipped with a charge-coupled device camera (1024×298 diodes), which is Peltier cooled to 243 K to reduce the thermal noise. A He-laser (Melles Griot) was used to excite the Raman scattering at 632 nm with a laser power of 1.4 mW. The following spectrometer parameters were used: microscope objective, 100; slit width, 200 μm

(spectral resolution, 2.5 cm^{-1}); integration time, 240 s per spectrum; and 20 averages.

XRD analysis was carried out using an URD-63 spectrometer with Cu-K_α radiation in the 5–70 2θ range by continuous scanning (2°/min). The integration time was set at 20 s. The POLYCRYSTAL software package [15] was used to refine the structure of the sample calcined in air at 623 K and He at 713 K. Additional XRD measurements were done at room temperature on a STOE STADI-P focusing monochromatic transmission diffractometer equipped with a Ge(111) monochromator and a position sensitive detector. Cu-K_α radiation was used. The phase analysis was performed with the STOE Win XPOW software package (version 1.06; Stoe Darmstadt, Germany) and with PowderCell (V 2.3; Bundesanstalt für Materialforschung und -prüfung (BAM) Berlin, Germany).

The particle size distribution was measured on a Coulter Counter TA-2 from Coultronics. The specific surface areas were determined by the BET method (Micromeritics).

The morphology and the size of the catalyst particles after spray-drying and during calcination was determined by scanning electron microscopy (SEM) analysis. SEM was conducted on a S 4000 FEG microscope (Hitachi). The acceleration voltage was set at 10 kV, the objective aperture was 30 mm, and the working distance was 10 mm.

High-resolution transmission electron microscopy (HRTEM) analysis was carried out on a CM 200 electron microscope (Philips) (point resolution, 0.2 nm; acceleration voltage, 200 kV) equipped with an EDX system (EDAX). For HRTEM analysis, the samples were prepared from suspensions of the powders in methanol. A drop of the methanol slurry was put on holey-carbon/copper grids.

Thermal analysis (TA) was performed with a STA 449C Jupiter apparatus (Netzsch). Flowing helium and air atmosphere were applied (the flow rate was set at 15 ml/min in both cases). The heating rate was set at 10 and 20 K/min. Mass spectrometric analysis (TG-MS) of the evolved gases was performed with an Omnistar quadrupole mass spectrometer (Pfeiffer Vacuum).

The sieve fraction between 0.4 and 0.6 mm of crushed pellets was used for the catalytic measurements. The catalytic tests were performed in a quartz tubular flow reactor (i.d. 4 mm). The catalyst (0.025–0.1 g) was diluted with quartz (1:10–1:4 by weight) to achieve better temperature control. Reaction mixtures of 4% C_3H_4O, 8% O_2, 20% H_2O, and the balance He with total flow rates between 0.2 and 2 ml/s were used for the catalytic measurements. The reactants and products were analyzed by an on-line gas chromatograph (Varian 3800) equipped with TCD and FID detectors. A Porapak-QS column (2 m × 1/8 IN, s.s.) and a 60/80 Carboxen 1000 column (15 FTs × 1/8 IN, s.s.) were employed for the analysis of permanent gases and organic substrates. The carbon mass balance was 100 ± 5%.

Table 1
EDX data of the MoVW mixed oxides activated at the indicated temperature

Elements (at%)	$T = 383$ K	$T = 623$ K	$T = 713$ K
V	18.9	21.2	24.4
W	10.1	11.1	7.3
Mo	70.9	67.7	68.3

3. Results and discussion

3.1. SEM

Fig. 1a shows a characteristic SEM image of catalyst particles after spray-drying. All particles are spherically shaped and have smooth surfaces. Their sizes range from 2 to 50 µm with main values lying between 5 and 10 µm. The shape and the size of the spherical particles did not change after the calcination in air of the spray-dried material at 623 K, but the observed morphology of the sample changed after heating at 713 K in helium or in air. These results are given in Figs. 1b and 1c. One can see that now the spherical particles consist of numerous smaller particles of regular shape and size ranging from 0.2 to 0.5 µm. The EDX results given in Table 1 show that the concentrations of the different elements slightly change with thermal treatment.

3.2. Particle size distribution and BET surface area

Analysis of particle size distribution shows that most particles have sizes between 5 and 10 µm (59.5%) and these data are in line with the SEM analysis. About 21% of the particles are smaller than 5 µm, and a few particles are larger than 10 µm (19%). After calcination at 623 and 713 K, the particle size distribution did not significantly change.

The specific BET surface area of the dried precursor was very low at 0.8 m^2/g; that of the calcined oxide was 4.1 m^2/g. These values are close to those reported for the industrial MoVW mixed-oxide catalyst [6–9].

3.3. TG-MS

The TA data of the spray-dried $Mo_{0.68}V_{0.23}W_{0.09}O_x$ sample, measured in flowing synthetic air, are shown in Fig. 2A. Four main mass losses are observed at 385, 545, 621, and 675 K. Differential scanning calorimetry (DSC) performed simultaneously with TA shows endothermic events at 385, 525, and 675 K and two exothermic effects at 563 and 621 K, which are similar to the mass losses as evident from the DTG trace. The first endothermic effect is associated with a mass loss of 3.5% in the TA. As seen from the MS traces, 33.4% of the total amount of water in the catalyst is released from the sample. Water, carbon dioxide, ammonia, and nitrogen oxides are released at the endothermic and exothermic effects at 525 and 563 K, respectively. The release of carbon dioxide is due to the decomposition of vanadyl oxalate. Nitrogen oxides are formed from the oxidation of ammonia and the reduction of the vanadium and

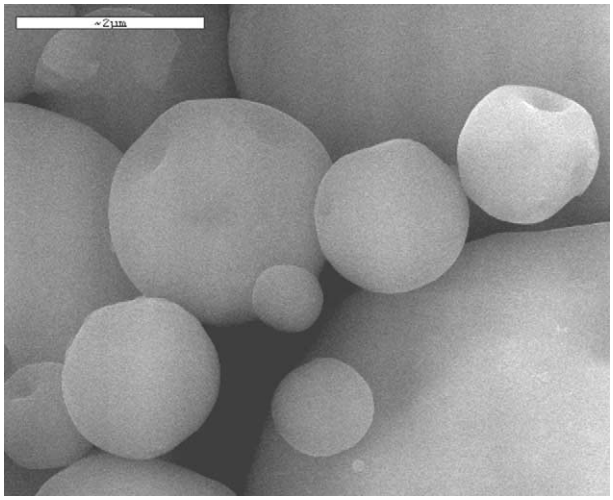

(a)

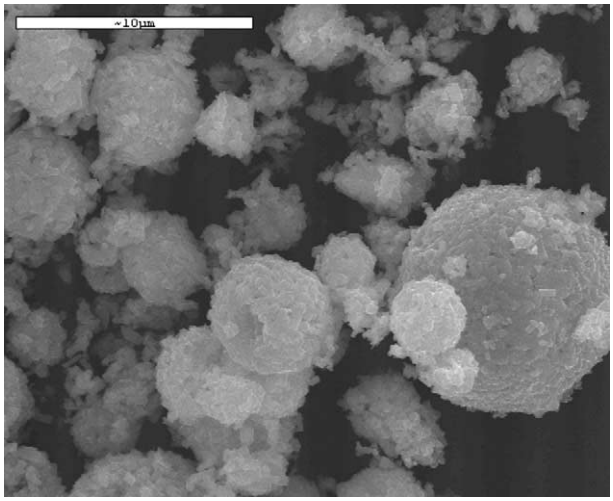

(b)

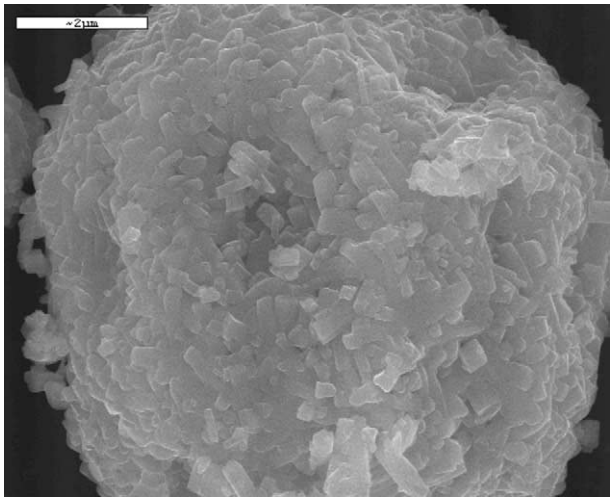

(c)

Fig. 1. Typical SEM images of the spray-dried precursor (a), the MoVW oxide catalyst heated at 623 K in air (b) and at 713 K in He (c) at different magnifications.

molybdenum precursors. An exothermic effect is detected at 621 K, which is related to only a slight mass loss of 3.5%. Water and traces of ammonia, carbon dioxide, and nitrogen dioxide are observed by MS. This exothermic effect is associated with a crystallization process as revealed by SEM and XRD.

Fig. 2B displays the TA data obtained in flowing helium of the sample which was pretreated in flowing air at 623 K for 2 h. Two major mass losses of 4.6 and 1.4% are observed. The DSC curve shows endothermic events at 378 and 555 K, which correlate with the mass losses as also confirmed by the DTG trace. The first effect is accompanied by a mass loss of 4.6% as shown in the TG curve. The MS analysis of the evolved gases shows that only water is released from the sample. The second endothermic effect at 555 K is also accompanied by loss of water. Other thermal effects or mass losses were not observed up to 743 K. In this experiment, the release of carbon dioxide or nitrogen oxides was not observed. These compounds obviously were completely released during the pretreatment of the precursor in air at 623 K for 2 h, in line with the TA data shown in Fig. 2A.

3.4. XRD

Fig. 3 displays the results of the XRD analysis of the $Mo_{0.68}V_{0.23}W_{0.09}$ mixed-oxide samples after the different treatment steps. The XRD patterns shown in Fig. 3 of the initial and calcined samples differ considerably. The XRD patterns reveal that the mixed $Mo_{0.68}V_{0.23}W_{0.09}$ oxide precursor was poorly crystallized after spray-drying (Fig. 3a) and after calcination in air at 623 K (Fig. 3b). The broad halo lying between 5° and 14° 2θ is characteristic for the XRD pattern of the spray-dried sample as evident from Fig. 3a. It should be noted that a set of reflections of the Mo_5O_{14} structure, such as (210) and (310), appear in this 2θ region (Figs. 3c and 3d). After thermal treatment of the spray-dried sample at 623 K in air, the halo disappeared and a broad XRD peak is observed at 22° 2θ in the XRD pattern of this sample (see Fig. 3b). In this case, the peak location is very close to that of the (001) reflection of Mo_5O_{14}. The spray-dried material shows a second broad signal at 27.6° 2θ. The broad reflection, observed in this range (Fig. 3a) transforms into a set of sharp peaks, including the (550) reflection of Mo_5O_{14}, after calcination in air at 723 K (Fig. 3c) and in air at 623 K plus in helium at 713 K (Fig. 3d). These observations indicate that a Mo_5O_{14}-type structure is preformed in the spray-dried precursor but of course with a very low degree of structural ordering within the basal plane. This observation is in agreement with published results of the structural studies of the nanocrystalline, industrial catalyst [6,16].

The XRD pattern of the MoVW sample calcined in air at the higher temperature of 723 K is shown in Fig. 3c. This temperature results in the crystallization of the complex Mo–V–W oxide of the Mo_5O_{14} type from the nanocrystalline, spray-dried material as confirmed by the appearance

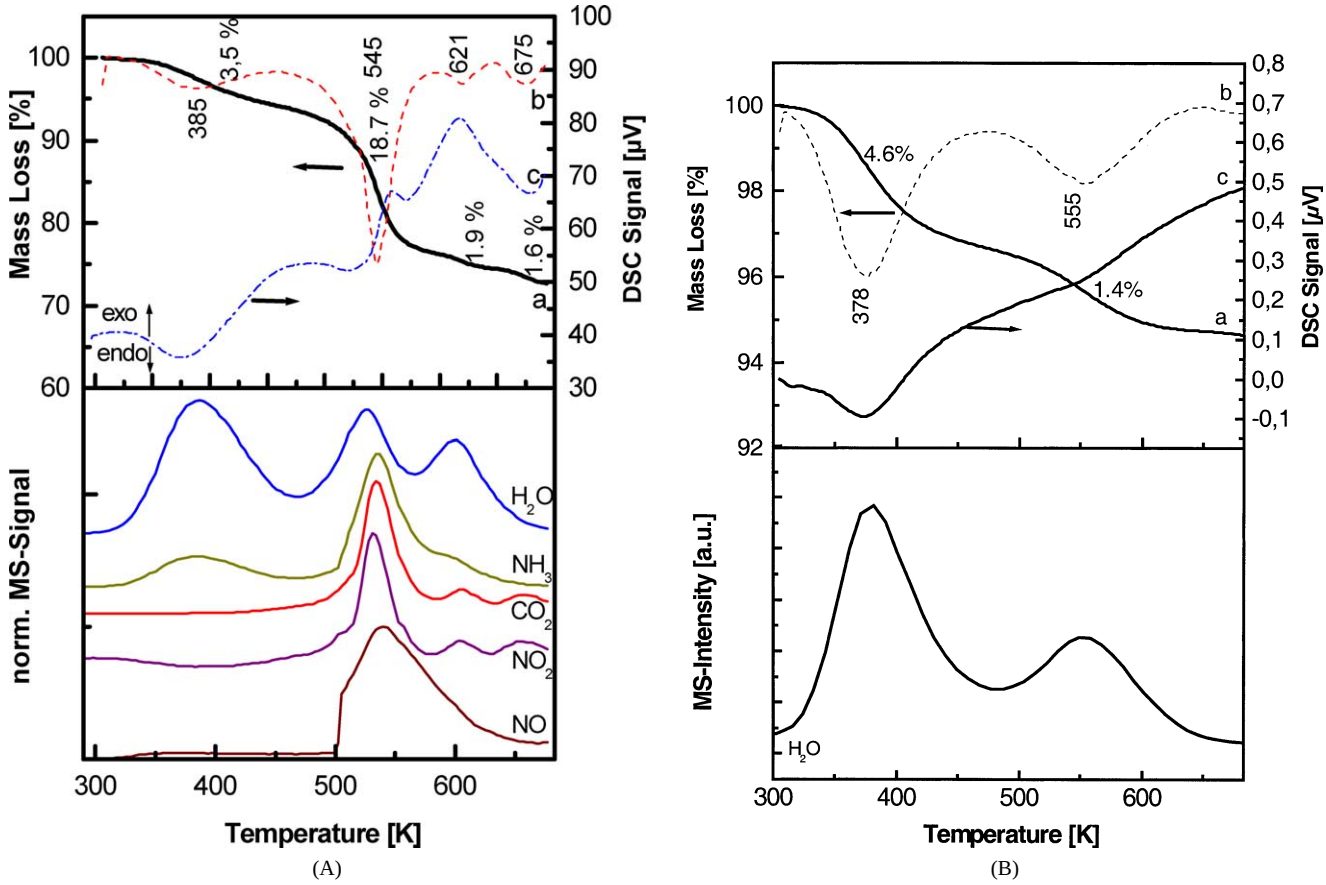

Fig. 2. (A) TA in flowing synthetic air of the spray-dried $Mo_{0.68}V_{0.23}W_{0.09}O_x$ catalyst. (Top) (a) TG data; (b) DTG data; (c) DSC data. (Bottom) MS traces of evolved H_2O, NH_3, CO_2, NO_2, and NO. (B) TA in helium of the spray-dried $Mo_{0.68}V_{0.23}W_{0.09}O_x$ catalyst pretreated in air at 623 K for 2 h. (Top) (a) TG data; (b) DTG data; (c) DSC data. (Bottom) MS trace of evolved water.

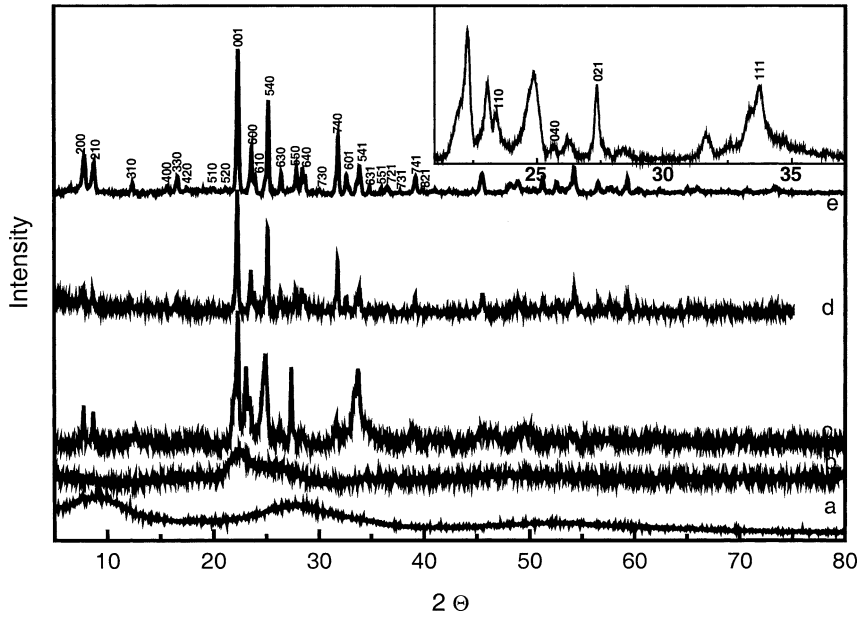

Fig. 3. X-ray pattern of the MoVW oxide precursor/catalysts. (a) Spray-dried precursor; (b) catalyst calcined in air at 623 K for 2 h; (c) catalyst calcined in air at 723 K for 2 h; (d) catalyst calcined in air at 623 K and in helium at 713 K; (e) catalyst calcined in air at 623 K for 2 h after operation in acrolein oxidation for 80 h. The inset shows the 2θ region of diffractogram c which shows reflections due to MoO_3.

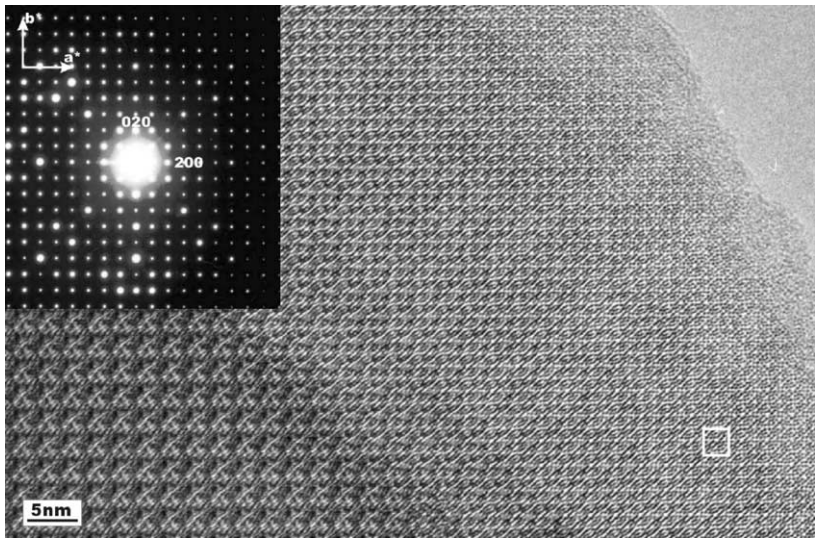

(a)

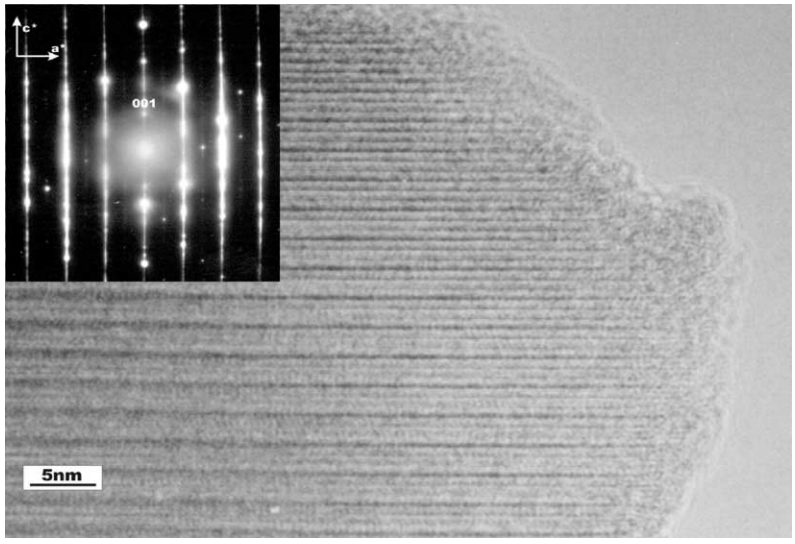

(b)

Fig. 4. HREM images and SAED patterns of Mo_5O_{14} structure viewed along the [001] (a) and [010] (b) directions.

of the sharp and characteristic peaks of this phase in the XRD diffractogram (Fig. 3c). However, traces of a MoO_3 phase are also detected for this sample. The inset of Fig. 3 shows the 2θ range of the diffraction pattern c, in which the reflections of MoO_3 occur as marked by their respective indices. The result of the assignment of the reflections are given in Table 2. These XRD data are corroborated by Raman spectroscopy (vide infra). Hence, the single-phase $Mo_{0.68}V_{0.23}W_{0.09}O$ compound of the Mo_5O_{14}-type structure could not be identified when the sample was heated in air at 723 K. MoO_3, known for its total oxidation activity, is definitely present in the catalyst.

The single-phase $Mo_{0.68}V_{0.23}W_{0.09}O$ compound of the Mo_5O_{14}-type structure is formed only after subsequently heating the catalyst, precalcined in air at the lower temperature of 623 K, in helium at 713 K, as evident from the XRD pattern of Fig. 3d, which additionally shows the in-

Table 2
X-ray data of the MoVW catalyst heated in air at 723 K

2θ	D	Int. (%)	Phase
7.77	11.4	32	$(MoVW)_5O_{14}$
8.69	10.17	29.9	$(MoVW)_5O_{14}$
12.30	7.19	10.5	MoO_3 (r)
15.6	5.68	8.4	$(MoVW)_5O_{14}$
22.29	4.0	100	$(MoVW)_5O_{14}$
23.13	3.84	55.2	$(MoVW)_5O_{14}$
23.44	3.79	39.0	$(MoVW)_5O_{14}$
24.82	3.58	39.4	$(MoVW)_5O_{14}$
27.28	3.266	36	MoO_3 (r)
31.66	2.824	17.1	$(MoVW)_5O_{14}$
33.74	2.66	32.8	MoO_3 (r)
38.98	2.31	12.2	$(MoVW)_5O_{14}$

dices of the reflections of $Mo_{0.68}V_{0.23}W_{0.09}O$. It has to be noted that the XRD pattern recorded for the catalyst, which was thermally treated in air at 623 K and then operated in the acrolein oxidation for 80 h (Fig. 3e), is similar to the pattern of Fig. 3d. This observation confirms recent results on the enhanced formation of the Mo_5O_{14}-type structure during acrolein oxidation [7].

The XRD pattern of Fig. 3d was used for the structural refinement of the ternary oxide sample. According to the results obtained, the structure is well described by the space group P4/nmm with the following lattice parameters: $a = 4.54063$, $b = 4.54063$, and $c = 0.39979$ nm. A slight decrease of the unit cell parameters of the thermoactivated ternary oxide is observed as compared to the reference Mo_5O_{14} reported by Kihlborg [10] (P4/mbm space group, $a = 4.5990$, $b = 4.5990$, and $c = 0.3936$ nm). The incorporation of V and W ions into the structure of this molybdenum oxide could be the reason for this. It was shown above that crystalline particles of this sample have W and V contents as high as 9 and 23 at%, respectively.

Data given in Fig. 3 may indicate that the structure of the spray-dried catalyst precursor exhibits only close-range order rather than nanocrystalline three-dimensional (3D) periodicity, because there is only one single halo in the XRD pattern, which disappears upon calcination with the simultaneous growth of the broad (001) reflection of nanocrystalline Mo_5O_{14} (Fig. 3b). In the case of nanocrystallinity, there should be several very broad peaks, instead of one single halo, whose intensities grow with raising calcination temperature due to the increasing degree of sample crystallinity. Hence, it seems likely that the structure of the spray-dried sample is characterized by some structural ordering in the layer plane but does not possess any periodicity in the perpendicular direction, e.g., along [001].

Moreover, the gradual increase of the intensity of the (001) reflection during the crystallization of the Mo_5O_{14}-type structure from an amorphous, spray-dried precursor indicates a lamellar or pseudolamellar character of this mixed oxide (Figs. 3b–3d). When the layers begin to pack into slabs, the 3D periodicity of the MoVW oxide becomes evident. That is also demonstrated by the increasing intensities of the basal reflections. The proposed structural model fits well with Raman spectroscopic data, which also indicate the presence of nuclei of the Mo_5O_{14} phase in the spray-dried material, and with TEM observations, which confirm the pseudolamellar character of the Mo_5O_{14} structure (vide infra).

Attention should also be focused on the fact that the crystallization process of the Mo–V–W oxide from the amorphous precursor is governed by a proper maintenance of the cation oxidation states during the thermal treatment steps to the final catalyst. According to the XRD analysis, calcination of the spray-dried precursor in an oxidizing medium, i.e., air, leads to the partial disintegration of the complex oxide phase of the Mo_5O_{14} type as proven by the reflections of MoO_3 in the XRD pattern (Fig. 3, inset). Hence, the treatment of the spray-dried precursor under well-chosen tempering or reaction conditions is a critical requirement for the synthesis of well-crystalline, single-phase Mo–V–W oxide (Figs. 3c–3e).

3.5. HRTEM

According to TEM, the particles of the spray-dried and the calcined sample (air, 623 K; helium, 713 K) are of platelet-like shape with sizes of about 200 nm in length and 10 nm in width. With the help of selected area electron diffraction (SAED) patterns, the structure of the sample was identified as a Mo_5O_{14} type. The SAED pattern oriented along [001] zone axis and given in the inset of Fig. 4a reflects the closely packed character of the Mo_5O_{14} structure in the basal plane. The SAED pattern shown in the inset of Fig. 4b displays a set of strips similar to those characteristic of lamellar materials. Thus, this ternary oxide can be considered pseudolamellar. These layers are alternating along the [010] direction. It is evident from the TEM observations that the (010) plane is the most developed plane of the crystalline particle.

At higher magnification, the structure of the sample is rather complicated. A cubic motif of the dark spots is clearly visible in the HRTEM micrograph of the sample, indicating the Mo_5O_{14}-type structure viewed along the [001] orientation (see Fig. 4a). The distance between two neighboring spots is equal to 2.25 nm, which fits well with half of the unit cell parameter of Mo_5O_{14}. This value also coincides with the distance between two channels formed by the pentagonal bipyramides in the structure of this complex ternary oxide [17,18]. Therefore, it can be suggested that the micrograph in Fig. 4a shows the channels in the basal plane. On the other hand, the pseudolamellar nature of the crystal structure is evident from the HRTEM image of the crystal viewed down the [010] projection (Fig. 4b) from which an interlayer parameter as long as 1 nm can be measured.

EDX measurements indicate similar elemental compositions for all investigated particles of the ternary oxide sample. As evident from EDX, the concentrations of Mo, V, and W are equal to 68.13, 22, and 9.88 at%, respectively. These values are in a good agreement with the EDX data obtained by SEM analysis.

The XRD and TEM data presented in this work are in a good agreement with earlier observations on the structural arrangement of the MoVW oxide with an admixture of MoO_3 [6,9]. The structural evolution of the main ternary phase during thermal treatment seems to be similar to the structural transformation of the catalyst in the present study. The XRD pattern of the precursor described in [6,9,16] shows the same diffuse peaks, which became sharp and strong due to crystallization of the initial structure upon thermal treatment. Note that the (210) and (200) reflections, although very broad, already exist in the XRD pattern of the precursor, whereas the (001) reflection is almost absent in the XRD diffractogram. After the first calcination step of the

precursor, the reverse situation was observed. The former reflections disappear, and the latter start to grow until the sharp and intense peaks appear after further heating. From the structural point of view, this implies that there is a kind of short-order and structural periodicity in the [210] direction, but it is very poor along the [001] direction. This finding is in line with recent TEM data [7,9], which indicated diffusion reflections in the SAED pattern. Irregular packing of thin layers within the ternary oxide particles in the direction perpendicular to the (001) basal plane leads to the so-called bundle structure. The TEM results obtained in this study also show this pseudolamellar character of the ternary MoVW phase.

3.6. Raman spectroscopy

Fig. 5A shows the Raman spectrum of an aqueous mixed solution of the three transition metal compounds and the spectra of individual AHM, AMT, and vanadyl oxalate solutions for comparison. The spectrum (a of Fig. 5A) of the pure, colorless AHM ($c = 0.96$ mol/l Mo) solution displays bands at 940, 894, 818, and 700 cm^{-1}, in agreement with literature [19]. The Raman spectrum of the pure, blue vanadyl oxalate solution ($c = 0.76$ mol/l V) displays bands at 974, 908, and 678 cm^{-1} (b of Fig. 5A), while a band is detected at 971 cm^{-1} for the pure, colorless AMT ($c =$ 0.27 mol/l W) (c of Fig. 5A). The spectrum d of Fig. 5A was recorded for the freshly mixed solution of the precursor solutions. Raman bands of the fresh mixed solutions are observed at 964, 944, 910, 821, 790, 711, and 682 cm^{-1}, which are in the typical regime for Raman bands of polyoxo metallates. These bands tentatively could be assigned to terminal M=O vibrations in the regime between 1 000 and 890 cm^{-1} and to M–O–M bridges in the regime between 890 and 600 cm^{-1}. The calculation of the theoretical spectrum of a hypothetical mixed solution, which was fitted to the experimental data (spectrum e of Fig. 5A), shows bands at 973, 940, 894, 817, 701, and 678 cm^{-1}. Note that the band positions and observed relative intensities of the different signals vary from those of the freshly mixed solution. This hypothetical sum spectrum is clearly different from that of the freshly mixed solution. Hence, it can be assumed that previously mixing the three starting solutions induces a chemical reaction toward a polyoxo compound on a Mo basis with incorporated V and W.

Fig. 5A f shows the spectrum of a freshly mixed solution, after additional heat treatment at 353 K for 1 h. The Raman spectrum of this solution (Fig. 5A b) also differs decisively from that of the freshly mixed solution (Fig. 6A e). A new intense band appears at 878 cm^{-1} together with bands at 697 and 683 cm^{-1}. These bands appear in the typical regime of frequencies of Me–O–Me bridge stretching modes. The observation of these bands, thus, points to the formation of polymeric aggregates after this additional heating presumably containing W and V due to the absence of their respective Raman bands in the spectrum.

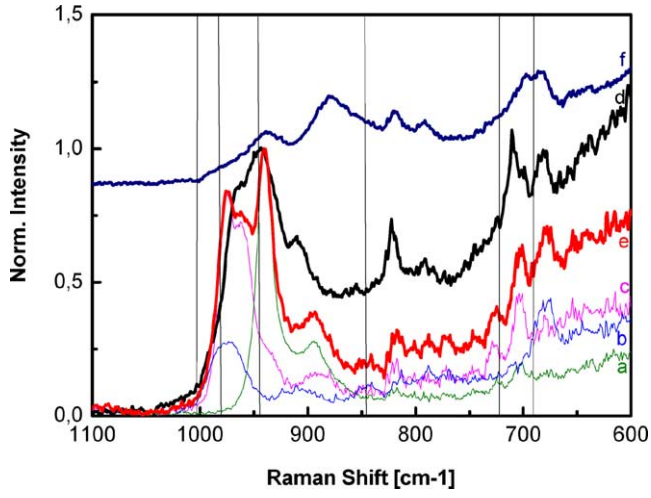

(A)

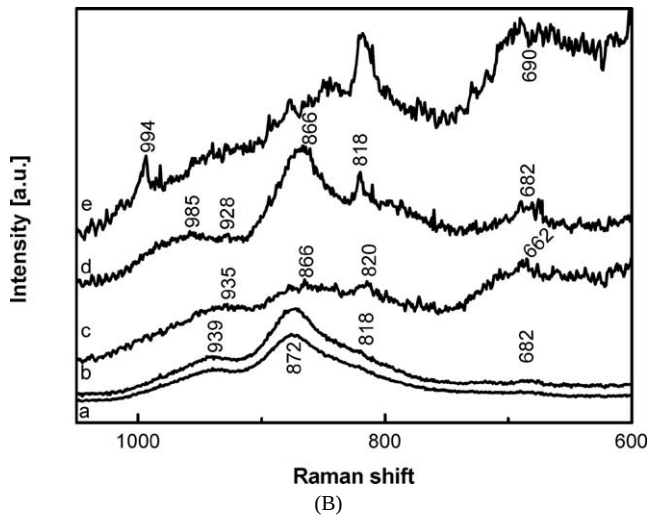

(B)

Fig. 5. (A) Raman spectrum normalized to the intensity of the band at 944 cm^{-1} of (a) the ammonium heptamolybdate solution, (b) the vanadyl oxalalate solution, (c) the ammonium meta tungstate solution, (d) the mixed solution (0.53 mol/L Mo; 0.18 mol/L V; 0.07 mol/L W), (e) the sum as calculated from the respective weighted spectra of the pure starting compounds and fitted to the experimental spectrum, and (f) the mixed solution (of d) after heat treatment at 353 K for 1 h. (B) Raman spectra of the MoVWO oxide precursor/catalysts: (a) spray-dried, (b) dried in air at 383 K overnight, (c) calcined in air at 623 K for 2 h, (d) calcined in air at 623 K for 2 h and in helium at 713 K for 2 h, and (e) heated in air at 723 K for 2 h.

The Raman bands, detected at 938 and 872 cm^{-1} in the solution Raman spectrum (Fig. 5A f) are also observed in the Raman spectrum of the spray-dried solid (Fig. 5B a) together with a broad wing extending to lower wavenumbers and a very weak band at 682 cm^{-1}. Simultaneously, all other bands that were recorded for the solution disappear. Spectral alterations are evident as compared to the solution Raman spectra (Figs. 5A and 5B). By comparison with Raman spectra reported for $Mo_{0.68}V_{0.23}W_{0.09}$ mixed-metal oxide catalysts [6,9], the band observed at 872 cm^{-1} after this treatment step is tentatively attributed to a mixed

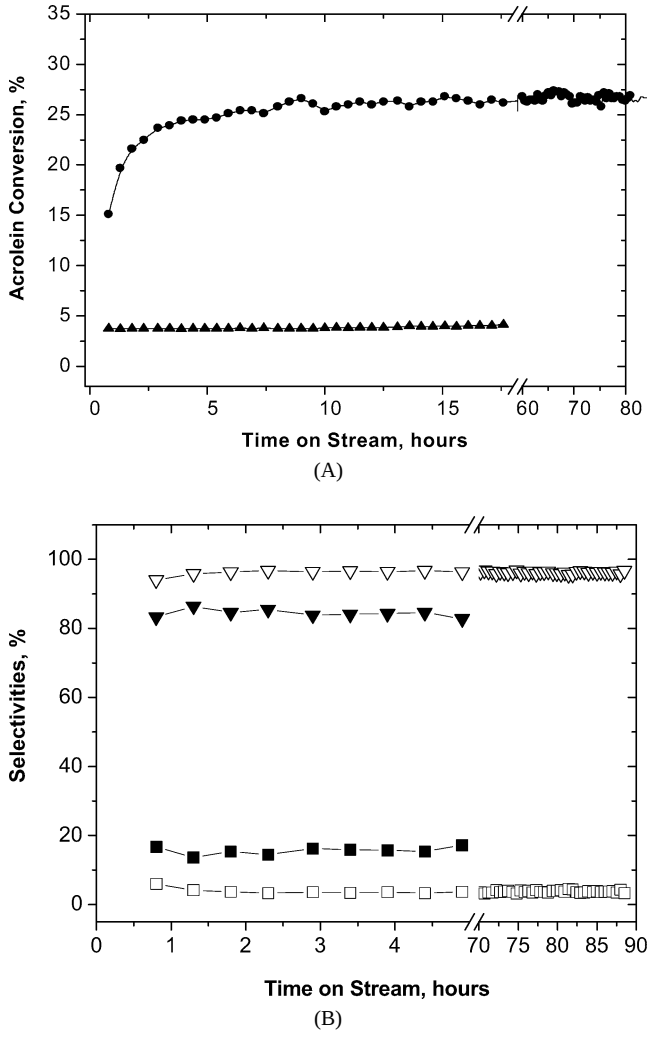

Fig. 6. (A) Acrolein conversion over the $Mo_9V_3W_{1.2}O_{14}$ catalyst at 563 K and as a function of operation time on stream. Spray-dried sample after calcination in air at 623 K for 2 h (circles); spray-dried sample after calcination in air at 623 K for 2 h and subsequent treatment in He at 713 K for 2 h (triangles). Reaction mixture composition: 4% C_3H_4O, 8% O_2, 20% H_2O, balance—He. (B) Selectivities to acrylic acid (triangles) and $CO + CO_2$ (squares): spray-dried sample after calcination in air at 623 K for 2 h (open triangles and squares); spray-dried sample after calcination in air at 623 K for 2 h and subsequent treatment in He at 713 K for 2 h (filled triangles and squares).

oligomeric species with a molecular structure which might already contain the structural motif of Mo_5O_{14}, i.e., the central pentagonal bipyramid surrounded by five octahedra [14]. In this context, it has to be mentioned that similar Raman spectral bands were reported for the Keplerates also containing the pentagonal bipyramids as a structural motif [20,21] Thus, the combined information from XRD and Raman spectroscopy indicate the presence of a molecular MoVW precursor species and the absence of long-range order in the spray-dried solid precursor. After further drying at 383 K overnight, the Raman spectrum (Fig. 5B b) of the sample has not changed. The relative intensity of the band at 866 cm^{-1} attributed to the polyoxo $(MoVW)_5O_{14}$ precursor, however, has increased somewhat compared to the band at the same wavenumber of the spectrum recorded in solution. A comparison with the XRD results (Fig. 3) clarifies that the X-ray amorphous spray-dried precursor consists of these polyoxo clusters. Calcination of the sample in air at 623 K for 2 h resulted in a Raman spectrum (Fig. 5B c) which has considerably altered as compared to the spectrum of the dried materials (Fig. 5B a). The formerly prominent bands between 800 and 1000 cm^{-1} have changed in shape and have lost their structure. The band at 662 cm^{-1} assigned to Me–O–Me bridges shows a higher relative intensity compared to the bands between 800 and 1000 cm^{-1}. This increased intensity might indicate an increased degree of cross-linking in the solid. However, the Raman spectrum is still poorly resolved and is additionally characterized by a high background extending to lower frequencies, which points to an ill-defined, poorly crystallized material, in line with the XRD results (see Fig. 3). The Raman spectrum of Fig. 5B d was recorded of the catalyst additionally tempered in He at 713 K for 2 h. The spectrum is more resolved compared to the spectrum of the preceding step and shows bands and shoulders at 985, 949, 866, 818, 682, and 584 cm^{-1}. The Raman bands are more resolved and the background is reduced compared to the mixed oxide after thermal treatment at 623 K in air. The observed band positions are in agreement with those reported by Dieterle et al. [9] and Blume [13] for the catalyst prepared by other methods and with a different transition metal ratio. These spectral alterations indicate an increase in crystallinity of the mixed oxide after this treatment step that fits well with the XRD results, which demonstrated the crystallization of the Mo_5O_{14}-type mixed oxide.

When the spray-dried sample was additionally calcined at 723 K for 2 h, Raman shows bands or shoulders at 995, 875, 845, 818, and 667 cm^{-1} (Fig. 5B f). The Raman band at 891 cm^{-1} can be attributed to monoclinic Mo_4O_{11} [22], whereas the band at 845 cm^{-1} may be assigned to orthorhombic Mo_5O_{14}, which is characterized by Raman bands at 983, 909, 845, 790, and 728 cm^{-1} [13]. But XRD did not reveal the presence of Mo_4O_{11} in the sample (see Table 2) which is likely to be caused by its XRD amorphous state. Obviously, calcination in air at temperatures below 673 K (data not shown) leads to the formation of $(MoVW)_5O_{14}$ in phase mixtures with traces of MoO_3. Temperatures higher than 673 K result in the decomposition of the majority of the $(MoVW)_5O_{14}$ phase into a broad phase mixture.

3.7. Catalytic properties

The catalytic performances of the different, above-described materials were studied in the acrolein oxidation under identical reaction conditions. Fig. 6A shows the acrolein conversions at 563 K and at $\tau = 0.12$ g s/ml as a function of time on stream. The selectivities to acrylic acid and $CO_2 + CO$ with time on stream are displayed in

Fig. 6B. It is evident from Figs. 6A and 6B that the precursor pretreatment in air or in air plus He considerably affected the final catalytic properties. The catalyst, calcined only in air at 623 K for 2 h, shows an activation period similar to that observed for an industrial MoVWO catalyst [7]. It is important to note that a significant change in catalytic performance was not observed during the first minutes of operation, which could be related to surface processes, such as desorption of water or surface reduction. Such processes can be excluded as responsible for the improving catalyst activities. Moreover, the BET surface areas of all materials were very low with about 4 m^2/g and did not change upon the different calcination treatments or catalysis. Textural changes, thus, can be excluded as responsible for the changing catalytic activity. As suggested in the previous work [7], such an activation period is related to the formation of an active crystalline phase. In full agreement and confirming previous results, XRD of the catalyst after operation in the acrolein oxidation for 80 h revealed the exclusive presence of crystalline $(MoVW)_5O_{14}$ in this sample (Fig. 3e). The selectivity to acrylic acid over the catalyst calcined in air also slightly increased with time on stream and reached 97% at an acrolein conversion of 25–26%, while that to $CO + CO_2$ decreased (Fig. 6B). This slight change in the selectivities over the first 1.5 h might be related to redox processes within the catalyst material [6]. However, it has to be stated that the time scale of the selectivity changes does not correlate with that of the increasing catalyst activity. Hence, this result once more proves that this increasing catalyst activity is not directly related to redox processes in the material, which should be reflected by selectivity alterations.

The steady state selectivity to acrylic acid of 97% finally reached is close to that of the industrial catalyst [7]. The catalyst, which was additionally treated in He at 713 K for 2 h, reached only a six to seven times lower acrolein conversion rate under identical reaction conditions. Its selectivity to acrylic acid was also lower at 86%.

It is important to emphasize that treatments which lead to the decomposition of the Mo_5O_{14}-type structure were not applied in the present catalytic tests. Previous investigations have demonstrated [9] that the Mo_5O_{14}-type structure is stable up to 818 K in He. Thermal treatments at temperatures above 829 K led to the decomposition of the metastable Mo_5O_{14} phase to stable MoO_3 and MoO_2 [9]. Additionally, strong oxidative or strong reductive conditions were not used in the present study, which also result in the formation of phases with higher or lower degrees of reduction, such as MoO_3 or Mo_2O_{5-x} [6,9,23].

XRD analysis on the sample with the high catalytic activity (sample heated in air at 623 K for 2 h) revealed that a crystalline Mo_5O_{14} structure appears after operation in the acrolein oxidation reaction (Fig. 3e). As was shown previously the structure of the sample before reaction represents poorly crystalline (almost X-ray amorphous) material. It seems likely that the induction period observed for this sample is caused by crystallization of the Mo_5O_{14} phase during the reaction. Note that the catalyst heated in air and in helium and composed of single crystalline Mo_5O_{14}-type structure shows low activity and less selectivity for acrolein despite identical XRD patterns of the activated material.

This phenomenon might be associated with different "real structures" of the compound under reaction conditions, e.g., size of the Mo_5O_{14} particles, degree of nanocrystallinity, and different oxidation states of molybdenum, vanadium, and tungsten. Further, the character of the structural disordering during the reaction might also be significant. This result shows the full complexity of the system by demonstrating that the long-range structure of a catalyst is necessary but by no means sufficient information to obtain a structure–function relationship. New ways in catalysis research are therefore recommended that investigate in detail the real structure of the material in situ under reactive conditions.

4. Conclusion

A synthesis procedure which allowed the preparation of the single-phase, well-crystallized Mo_5O_{14}-type oxide has been developed in this work. The whole process of structure formation starting from the precursor solutions up to the final product has been closely monitored. A strong interaction of AHM, AMT, and vanadyl ions involving the formation of Me–O–Me bridges and a mixed Mo, V, W compound was observed with a structure closely related to that of the Mo_5O_{14} type. This structural motif was maintained during the spray-drying process but the material showed a low crystallinity. Further thermal treatment removed ammonia, water, and oxalate and increased the state of crystallinity. While calcinations in air led to overoxidation with a phase mixture among a well-crystallized Mo_5O_{14}-type structure, the pure single phase was obtained only after additional treatment in helium.

Particles of this Mo_5O_{14}-type compound are oriented along the [001] and the [010] zone axes. Microdiffraction patterns show the closely packed character of the Mo_5O_{14}-type structure in the basal plane. This ternary oxide is pseudolamellar with alternating layers along the [010] direction and a strongly developed (010) face. Structure refinement showed decreased **a** and **b** lattice parameters with respect to Kihlborg et al. [10], but an increased **c** parameter. This effect is probably due to incorporation of V and W into the lattice. This statement is also supported by Raman spectral features and shows the importance of V and W as structural promoters to maintain the Mo_5O_{14}-type phase, presumably by stabilizing the pentagonal bipyramides.

While the catalyst that formed the Mo_5O_{14} structure after an induction period of about 2.5 h achieved the highest catalytic activity for acrolein oxidation, the synthesized single-phase material showed less activity but its selectivity was almost as high as that of the industrial material. Some

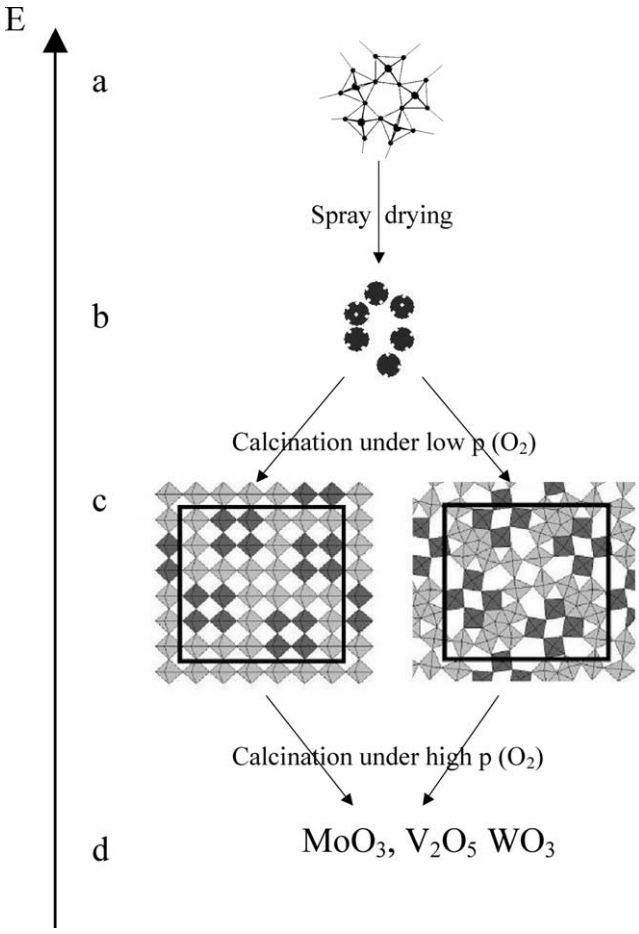

Scheme 1. (a) Oligo anions in solution; (b) material after spray-drying (with oxygen defects); (c) material calcined under low oxygen partial pressure where a variety of defects can be obtained; (d) binary oxide materials calcined under higher oxygen partial pressure (i.e., air).

important conclusions can be drawn from this. Apparently the active material is single phase but distinctively different from the perfect structure of Mo_5O_{14}. The Mo_5O_{14} structure is an idealized endpoint that is formed under reduced oxygen partial pressure by the organization process of a mixture of oligo anions, which are generated in solution. The active phase is metastable until crystallization and oxidative decomposition into binary oxide phases occurs under high oxygen partial pressure (air and above). This is illustrated in Scheme 1.

These experimental results are highly significant for future catalysis research, because they confirm that a single-phase material can be catalytically active and that no phase cooperation or spill over phenomena are functionally essential. Additionally, this work has highlighted the full complexity of these systems, because X-ray powder diffractometry indicates the same crystallographic phase for two differently active materials. This difference can be explained only by different "real" structures of the two materials. It must be strongly emphasized that precise analytical methods that reveal the details of a real structure of a given phase need to be developed to determine structure–function relationships. The synthesis procedure reported in this paper is an example of this approach.

References

[1] A.N. Kurtz, R.W. Cunningdam, A.W. Naumann (Union Carbide Co.), US Patent 4111983, 1978.
[2] V. Novak, L. Sokol, J. Jelinek, CS 1207807 B, 1981.
[3] N. Bertolini, S. Ferlazzo (Euteco Impianti S. p.A.), US Patent 4289654, 1981.
[4] T. Kawajiri, S. Uchida, H. Hironaka (Nippon Shokubai Kagaku), EP 427 508 A1, 1991.
[5] A. Tenten, F.-G. Martin, H. Hibst, L. Marosi, V. Kohl (BASF AG), EP 668104 B1, 1995.
[6] G. Mestl, Ch. Linsmeier, R. Gottschall, M. Dieterle, J. Find, D. Herein, J. Jäger, Y. Uchida, R. Schlögl, J. Mol. Catal. A 162 (2000) 455–484.
[7] O. Ovsitser, Y. Uchida, G. Mestl, G. Weinberg, A. Blume, M. Dieterle, H. Hibst, R. Schlögl, J. Mol. Catal. A 185 (2002) 291–303.
[8] M. Dieterle, PhD thesis, TU Berlin, 2001.
[9] M. Dieterle, G. Mestl, J. Jäger, Y. Uchida, R. Schlögl, J. Mol. Catal. A 174 (2001) 169–185.
[10] L. Kihlborg, Ark Kemi 21 (1963) 427.
[11] T. Ekström, M. Nygren, Acta Chem. Scand. 26 (5) (1972) 1827–1835.
[12] T. Ekström, M. Nygren, Acta Chem. Scand. 26 (5) (1972) 1836–1842.
[13] A. Blume, PhD thesis, Berlin, 2002.
[14] G. Mestl, J. Raman Spectrosc. 33 (2002) 335–347.
[15] L.P. Solovyeva, S.V. Tsybulya, G.N. Kryukova, E.M. Moroz, JSTCAM 32 (1991) 18.
[16] H. Werner, O. Timpe, D. Herein, Y. Uchida, N. Pfaender, U. Wild, R. Schlögl, H. Hibst, Catal. Lett. 44 (1997) 153.
[17] L. Kihlborg, Acta Chem. Scand. 26 (1972) 3381.
[18] W. Ueda, K. Oshihiara, Appl. Catal. A 200 (2000) 135–143.
[19] G. Mestl, T.K.K. Srinivasan, Catal. Rev.-Sci. Eng. 40 (4) (1998) 451–570.
[20] A. Müller, S. Polarz, S.K. Das, E. Krickemeyer, H. Bögge, M. Schmidtmann, B. Hauptfleisch, Angew. Chem. 111 (1999) 3443–3493.
[21] A. Müller, S. Sarkar, S.Q.N. Shah, H. Bögge, M. Schmidtmann, S. Sarkar, P. Kögerler, B. Hauptfleisch, A.X. Trautwein, V. Schünemann, Angew. Chem. 111 (1999) 3435–3439.
[22] A.A. Bolznan, B.J. Kenned, C.J. Howard, Austr. J. Chem. 48 (1995) 683.
[23] Y. Uchida, G. Mestl, O. Ovsitser, J. Jäger, A. Blume, R. Schlögl, J. Mol. Catal. A 187 (2002) 247–257.